PHYSICAL REVIEW C VOLUME 16, NUMBER 5 NOVEMBER 1977

Isobaric yield curves at $A = 72$ from the spallation of molybdenum isotopes by high-energy alpha particles

Thomas H. Ku* and Paul J. Karol
Department of Chemistry, Carnegie-Mellon University, Pittsburgh, Pennsylvania 15213
(Received 12 May 1977)

Absolute yields of 18 products with $65 \leq A \leq 76$ have been measured for the interaction of 720-MeV α particles with enriched ^{92}Mo, ^{96}Mo, and ^{100}Mo. Isobaric yield (charge dispersion) curves have been constructed for $A = 72$ to examine the effect of target neutron-to-proton composition on spallation product formation. Results indicate that isobaric yield curve peak positions are moderately dependent and asymmetric shapes strongly dependent on target N/Z, the latter particularly so for neutron-richer products. Comparisons with proton results and empirical predictions are presented.

[NUCLEAR REACTIONS ^{92,96,100}Mo(α, spallation), $E_\alpha = 720$ MeV; cross sections for 18 products $65 \leq A \leq 76$; constructed isobaric yield curves at $A = 72$. Enriched targets, Ge(Li) detectors, radiochemistry.]

I. INTRODUCTION

Studies of high-energy spallation reactions have yielded valuable information on reaction mechanisms and nuclear properties. Results of these studies have many important applications in other fields.[1,2] For instance, spallation cross sections provide the basis for understanding the composition of cosmic-ray nuclei, as well as radioisotope concentrations in meteorites and on the lunar surface. Practical utilization of the spallation process for production of radioisotopes, such as in nuclear medicine, requires spallation cross sections which are essential for determining the appropriate targets and purification requirements.[3,4]

The general mechanism by which high-energy spallation reactions have been described is based on Serber's cascade-evaporation model.[5,6] This model presents the spallation reaction as a two-step process. The first step is fast (10^{-22} sec) during which the incident high-energy projectile initiates a knockon cascade inside the nucleus and ejects a number of fast particles from the target nucleus, leaving behind an excited residual nucleus. The second step is relatively slower, typically about 10^{-16}–10^{-20} sec, during which the residual nucleus is deexcited by evaporation of nucleons or clusters of nucleons. The final product is obtained when the amount of excitation energy left in the nucleus is no longer sufficient to evaporate further nucleons. The cascade process usually leads to a diversity of excited residual nuclei, each with a spectrum of excitation energies. These nuclei in turn produce a broad distribution of final spallation products.

An important method for studying spallation reactions has been the measurement of the formation cross sections for products with the same mass number. Detailed knowledge of the distribution of yields among isobars is required for the construction of the yield-versus-mass curve and the determination of total inelastic cross sections from analysis of which further understanding of the details of the spallation reaction mechanism can be acquired.

In their 1959 review article, Miller and Hudis[7] noted that the relative yields of a number of isobars for spallation reactions are essentially independent of projectile energy and target mass. They suggested that target composition is relatively unimportant to the final *distribution* of the spallation products although the total isobaric yields do depend on target. Any difference in the initial conditions will be washed out during the evaporation phase of the reaction. These observations by Miller and Hudis, were, however, based on the results obtained from interactions with relatively light targets which lie very close to the stability line of the nuclide chart. That is, the targets all have very similar neutron-to-proton ratios (N/Z).

The conjecture that target composition would affect the relative yields among isobars was first introduced by Dostrovsky, Rabinowitz, and Bivins.[8] Based on their theoretical calculations using the Monte Carlo method, they predicted that by changing the position of the initial nuclide with respect to stability, the relative isobaric yields would be altered. This prediction seemed to agree with later observations by Kaufman,[9] who investigated the charge distributions of products in the mass range 66–74 from the irradiations of In, Au,

and U with 2.9-GeV protons. Kaufman found that the isobaric yield ratios are dependent on the target mass, with the heavier targets favoring the formation of neutron-rich nuclides. However, since the reactions involved included fission for U and Au, no conclusion was drawn about Miller and Hudis's[7] hypothesis of invariant isobaric yield distribution.

Later work carried out by Porile and Church[10] provided a definitive answer to this question. They examined the isobaric yield curves at $A \simeq 72$ from the bombardments of ^{96}Zr, ^{96}Mo, and ^{96}Ru with 1.8-GeV protons and reported that the isobaric yield distribution depended strongly on the N/Z value of the target nucleus. The most probable yield at $A = 72$ shifted toward more neutron-rich products in going from ^{96}Ru to ^{96}Zr, causing the yields to change markedly from target to target. Final spallation products retained a memory of target nucleus composition if the targets were sufficiently different in their N/Z values. Similar correlation between the yield distribution and the target N/Z value was subsequently revealed by the results of many other investigations.[11-16]

These previous investigations on isobaric yields were all performed using protons as the incident particle. Therefore, it seemed desirable to undertake a detailed study using α particles as the incident particle. The yield patterns of high-energy nuclear reactions induced by protons and α particles have been shown experimentally to be very much the same, the main difference being a greater yield by a factor of about 2 in the case of α particles.[17-19] The results of the present study, when compared with proton results, may reveal some specific differences in the interactions of the two types of particles possibly leading to further insight into the details of the reaction mechanism. The target nuclides employed in this work were ^{92}Mo, ^{96}Mo, and ^{100}Mo. The large differences in their N/Z values make them particularly suitable for this study.

In the present work, the yields of the $A = 72$ isobars were measured. This mass chain is sufficiently far away from the targets so that the yields are entirely due to spallation as opposed to simpler reactions which are markedly influenced by nuclear structural details of the target.[20-23] It also has the advantage of having four radioactive isobars with relatively long half-lives and well-studied decay schemes. Four cross sections, however, were not quite sufficient to describe an isobaric yield curve (^{72}Ge is stable) completely. To assist in the curve delineation, the yields for 14 other nuclides in the neighboring mass chains ($A = 65-76$) were combined, with appropriate corrections for dependence on mass yield.

II. EXPERIMENTAL

All bombardments were performed using the synchrocyclotron at the Space Radiation Effects Laboratory (SREL),[24] Newport News, Virginia, utilizing the internal 720-MeV α beam. The stacked foil activation method was employed. The number of α particles (including multiple traversals) striking the target was monitored by the ^{27}Al$(\alpha, X)^{24}$Na reaction. Irradiations were typically 10 min in duration for absolute cross section measurements and 1–3 h for relative yield determinations (e.g., ^{72}Zn, ^{66}Ge). Activated targets were usually brought back to Carnegie-Mellon University for chemical separation and radiation assay.

The targets used in this study were made from (>96%) enriched powder of ^{92}Mo, ^{96}Mo, and ^{100}Mo isotopes by a previously described sedimentation-pressing technique[25] in which an enriched isotope sediment on a 12.7-μm aluminum backing together with three more 12.7-μm Al foils were simultaneously pressed and trimmed into a 1.50-cm $\times$ 2.00-cm sandwich by a hydraulic press under a pressure of approximately 20 tons. The pressing process compressed the Mo powder into a dense layer and caused it to be physically bound to the two inner Al foils at the Al-powder interfaces. The two outer Al foils in the sandwich served as beam monitors. After pressing, the target sandwich was wrapped in a 12.7-μm Al guarding envelope. In this study, 5–8-mg/cm^2 target material was used. The quality of the targets was verified with scanning electron microscopy and β radiography, as described in Ref. 25.

For radiochemical separations, the target sandwich (Mo powder layer plus Al catcher foils) was dissolved in a mixture of hot concentrated H_2SO_4 and H_2O_2 which contained carriers of Ge, Se, As, Cu, Ga, and Zn (~10 mg each). Separation and purification schemes were modifications of previously formulated techniques.[9,26] The target solution was first made 5 M in HCl and germanium distilled in a stream of Cl_2 gas. Selenium and arsenic were distilled in HBr. Selenium was separated from arsenic by precipitation with SO_2. The residue solution was made 1 N in HCl and copper precipitated with H_2S. After a Mo_2So_3 scavenge, gallium was isolated by ether extraction. Finally, zinc was separated by ion exchange.

Since the ^{72}Zn and ^{66}Ge cross sections proved to be particularly small, special runs with long bombardment times were performed to obtain the activities of ^{72}Zn (relative to ^{65}Zn) and ^{66}Ge (relative to ^{69}Ge). After irradiation, Ge was separated from the target solution by distillation. Zn was extracted at pH 7.5 into dithizone (with diethanoldi-

thiocarbamate as masking agent) followed by back extraction into HCl.[27]

Chemical yield determinations were done by standard gravimetric methods and occasionally confirmed by spectrophotometric methods.[28] Yields were typically 60–70%.

The relevant properties of nuclides studied in this work and the detection methods used are listed in Table I. The decay of each nuclide was followed over a sufficiently long period to ascertain that it decayed with the proper half-life. The decay curves were analyzed by means of the Brookhaven decay curve analysis computer program (CLSQ)[29] to obtain the end-of-bombardment or time-of-separation activities and their standard deviations. ^{24}Na from the ^{27}Al$(\alpha, X)^{24}$Na monitor reaction was assayed with a calibrated β proportional counter.

III. RESULTS

All experimental cross sections were measured relative to the ^{27}Al$(\alpha, X)^{24}$Na monitor reaction. The value employed for the cross section of this reaction, 20.9 ± 2 mb at 720 MeV, was obtained from Karol[18] whose data also indicated that the contribution to the measured ^{24}Na activity from low-energy secondary particles in the target was negligible for the target thicknesses employed in this study.

The experimentally determined spallation cross sections are presented in Table II. Each yield is identified as being either independent (I) or cumulative (C), and is the average of several separate determinations listed in parentheses following each value. In column 2, the neutron-to-proton ratio of each product nuclide is given. The uncertainty associated with each cross section represents total experimental uncertainty, which is the combination of the random and systematic uncertainties. The sources of random uncertainties included counting statistics and decay curve analyses, chemical yield, parent-daughter separation time, and target misalignment. The primary areas of systematic uncertainty were counter efficiencies, decay schemes, summing corrections, and corrections for minor isotopic impurities in the target. Separate studies with the counting geometries employed showed that angular correlation effects on the summing phenomenon could be safely neglected. The decay scheme[30] of ^{73}Se^m represents a special case: 27% of the ^{73}Se^m (42 min) formed in the reaction decays directly into ^{73}As without going through its ground state ^{73}Se^g. Therefore the observed cross section of ^{73}Se is actually (^{73}Se^g + 73% ^{73}Se^m) because measurements were performed after the

TABLE I. Relevant properties of nuclides measured. (Except where noted, all properties were taken from Ref. 44.)

Nuclide	Half-life	Radiation measured (keV)	Branching abundance	Method of detection[a]
^{67}Cu	61.7 h	γ (184)	0.40	Ge(Li)
^{65}Zn	244 day	γ (1115)	0.507	Ge(Li), NaI
^{72}Zn	46.5 h	γ (145)	0.850[b]	Ge(Li), NaI
^{66}Ga	9.5 h	γ (1039)	0.372	Ge(Li)
^{67}Ga	78 h	γ (184)	0.24	Ge(Li)
^{72}Ga	14.10 h	γ (630)	0.252	Ge(Li)
^{66}Ge	2.27 h	^{66}Ga		Daughter
^{68}Ge	287 day	Ga K x ray	0.37[c]	Thin Ge
^{69}Ge	39.2 h	γ (573), x ray	0.14	Ge(Li), thin Ge
^{71}Ge	11 day	Ga K x ray	0.37[c]	Thin Ge
^{71}As	62 h	γ (175)	0.911[d]	Ge(Li)
^{72}As	26.0 h	γ (834)	0.800[b]	Ge(Li)
^{73}As	80.3 day	γ (53)	0.10	Ge(Li)
^{74}As	17.77 day	γ (596)	0.592	Ge(Li)
^{76}As	26.32 h	γ (559)	0.410	Ge(Li)
^{72}Se	8.4 day	^{72}As		Daughter
^{73}Se	7.2 h	γ (360)	0.953	Ge(Li)
^{75}Se	120 day	γ (136)	0.161	Ge(Li)
^{24}Na	15.0 h	β (1390)	1.00	β prop.

[a] The symbols used in this column have the following meaning: Ge(Li) = Ge(Li) detector, NaI = 7.6- × 7.6-cm NaI(Tl) detector, thin Ge = thin Ge x-ray detector, β-prop. = end-window gas-flow proportional counter.

[b] Reference 34.

[c] Calculated from information in Ref. 33.

[d] Reference 35.

TABLE II. α spallation cross section (mb) at 720 MeV.

Nuclide (I or C)[a]	N/Z	^{92}Mo	^{96}Mo	^{100}Mo
^{67}Cu (C)	1.310	0.055 ± 0.005(4)	0.190 ± 0.015(4)	0.334 ± 0.041(3)
^{65}Zn (C)	1.167	10.01 ± 0.97(4)	5.50 ± 0.45(4)	2.02 ± 0.33(3)
^{72}Zn (C)	1.400	(1.24 ± 0.24) × 10^{-4}(3)	(2.33 ± 0.36) × 10^{-4}(4)	(9.7 ± 1.7) × 10^{-3}(3)
^{66}Ga (I)	1.129	7.53 ± 0.70(4)	3.40 ± 0.26(4)	1.02 ± 0.09(3)
^{67}Ga (C)	1.161	13.3 ± 1.5(4)	6.34 ± 0.50(4)	2.75 ± 0.22(3)
^{72}Ga (I)	1.323	0.028 ± 0.003(4)	0.184 ± 0.017(4)	0.345 ± 0.032(3)
^{66}Ge (C)	1.063	0.421 ± 0.078(3)	(7.5 ± 1.3) × 10^{-2}(2)	(1.33 ± 0.27) × 10^{-3}(2)
^{68}Ge (C)	1.125	9.01 ± 1.13(4)	3.67 ± 0.32(4)	1.24 ± 0.16(3)
^{69}Ge (C)	1.156	13.4 ± 1.7(4)	6.26 ± 0.71(4)	2.61 ± 0.33(3)
^{71}Ge (I)	1.219	4.85 ± 0.72(4)	5.23 ± 0.44(3)	4.48 ± 0.38(3)
^{71}As (C)	1.152	16.8 ± 1.7(4)	7.99 ± 0.68(4)	3.24 ± 0.31(3)
^{72}As (I)	1.182	13.1 ± 1.4(4)	8.20 ± 0.87(4)	5.23 ± 0.55(3)
^{73}As (I)	1.212	8.85 ± 1.13(4)	7.22 ± 0.92(4)	5.96 ± 0.84(3)
^{74}As (I)	1.242	2.39 ± 0.21(4)	4.19 ± 0.35(4)	4.28 ± 0.36(3)
^{76}As (I)	1.303	0.116 ± 0.013(4)	0.474 ± 0.040(4)	1.12 ± 0.09(3)
^{72}Se (C)	1.118	10.3 ± 1.1(4)	3.34 ± 0.35(4)	1.31 ± 0.13(3)
^{73}Se (C)	1.147	18.9 ± 2.4(4)	8.00 ± 1.02(4)	3.89 ± 0.49(3)
^{75}Se (C)	1.206	32.3 ± 3.5(4)	18.5 ± 2.0(4)	11.5 ± 1.3(3)

[a] I, independent; C, cumulative.

^{73}Se^{m} was essentially gone, while the observed "independent" cross section of ^{73}As is (^{73}As + 27% ^{73}Se^{m}). No convenient way existed for determining the relative yield of the ^{73}Se^{m}/^{73}Se^{g} pair to make the appropriate correction. Thus an additional 5% and 10% maximum estimated uncertainty was assigned to the cross sections of ^{73}As and ^{73}Se, respectively, to account for this fact. However, the actual error is probably less than this since the isomeric state ^{73}Se^{m} has a low spin ($\frac{1}{2}$) and therefore probably a much lower formation cross section than the high spin ($\frac{7}{2}$) ground state according to the general trend observed in existing isomeric yield ratio measurements in other spallation systems.[31,32] The uncertainty in the monitor reaction cross section was not reflected in the quoted errors.

A. Isobaric yield curves

The isobaric yield curve, which shows the dependence of yield on nuclear charge at a particular mass number, is usually constructed by plotting the cross sections of the isobars as a function of N/Z, the neutron-to-proton ratio of the nuclide, or $Z - Z_A$, the difference between the charge of the nuclide and the most stable charge associated with isobars of mass A. The experimental cross sections, including those for the nuclides with masses other than 72, have been correlated to derive isobaric yield curves at $A = 72$. In deriving these curves N/Z was chosen as abscissa for convenience and the following approximation was assumed valid: The *shape* of the yield versus N/Z distribution along a mass chain remains unchanged for comparisons of close mass chains in the region $65 < A < 76$. This assumption is believed reasonable in view of the narrow mass region studied and justified by data from previous proton studies.[9,10,26] The isobaric yield curves in this region are thus considered identical except for shifts in absolute magnitude.

The use of cross sections spanning a range of mass numbers to construct a particular isobaric yield curve requires some knowledge of the total isobaric yield behavior over this mass range. The total isobaric yield (mass yield) of spallation products decreases nearly exponentially with increasing mass difference between the target and products. All data points are then corrected so as to coincide with the "$A = 72$ curve" by multiplying each yield by the factor $\exp[-p_x \cdot (A - 72)]$. In this work, the mass-yield coefficient p_x was calculated from the estimated total isobaric yield at $A = 67$ and $A = 72$. These two mass chains were chosen because the major portion of their total isobaric yields was experimentally observed. The estimated independent yields were obtained by requiring that a smooth curve be drawn through the interpolated and extrapolated independent yields such that their sums approximate as best as possible the measured cumulative yields. The total yield determined by this approach, together with the contribution of the directly observed cross section and the portion estimated from the curves, are summarized in Table III. An error equal to 20% of an interpolated yield was combined with the error of the measured yield to give the uncertainty

TABLE III. Total and interpolated cross sections (mb) at $A = 67$ and $A = 72$.

Target	^{92}Mo		^{96}Mo		^{100}Mo	
Mass number	67	72	67	72	67	72
Measured cross section	13.40 ± 1.46	23.45 ± 1.75	6.53 ± 0.50	11.72 ± 0.94	3.09 ± 0.22	6.89 ± 0.56
Interpolated cross section	2.50 ± 0.50	1.50 ± 0.30	2.60 ± 0.52	2.90 ± 0.58	2.80 ± 0.56	3.10 ± 0.62
Total cross section	15.90 ± 1.54	24.95 ± 1.77	9.13 ± 0.72	14.62 ± 1.10	5.89 ± 0.60	9.99 ± 0.84
Mass-yield coefficient p_x	0.090 ± 0.023		0.095 ± 0.020		0.106 ± 0.024	

of the total isobaric yield. It is seen that the total isobaric yield decreases by about 40% between $A = 72$ and $A = 67$ for the three target systems studied. Also listed in the table are the mass-yield coefficient p_x and its uncertainty. The value of p_x corresponds to a ~10% correction for each unit of mass-yield variation. This magnitude is comparable with the results obtained by Karol[18] for α spallation of Cu and less than those obtained by Cumming *et al.*[36,37] for high-energy proton, ^{12}C and ^{14}N spallation of Cu. The latter is consistent with Cumming's recognition of p_x as a "nuclear thermometer," larger values corresponding to lower deposition energies.[37] The uncertainties in p_x result in a 2.1–2.7% error in the correction for the change of one mass unit.

After the mass-yield corrections had been applied to all data a preliminary curve was drawn through the independent yields to give a first approximation of the isobaric yield distribution. Based on this curve, the cumulative cross sections were corrected for precursor contributions. A refined curve could then be plotted with the aid of these estimated independent yields. By repeating this procedure until further adjustments no longer introduced perceptible changes, more accurate corrections for the cumulative yields were accomplished. The conversion of cumulative yield to independent yield varied greatly in certainty depending on whether precursors lay on the peak or the wing of the curve. For example, the correction for ^{66}Ge was done with little uncertainty since its precursor falls on the lower end of the wing. On the other hand, the estimated independent cross section of ^{75}Se entails an appreciable uncertainty since its precursor is located on the peak of the curve causing the correction to be as high as 70%. In this work, the uncertainty associated with this correction procedure was assigned as 20% of the correction itself.

The corrected cross sections of the various products are plotted in Fig. 1 against N/Z for each of the three targets. The error bar associated with each point reflects the total experimental uncertainty (Table II) including the uncertainties in the applied corrections. As expected, the yields from the ^{92}Mo target are the highest among the three because of the shortest mass difference between target and products. The isobaric yield distributions are all peaked on the neutron-deficient side of the stability valley (^{72}Ge is stable) consistent with the general characteristics of the spallation mechanism.[2,7,38]

Although there is no *a priori* reason for the iso-

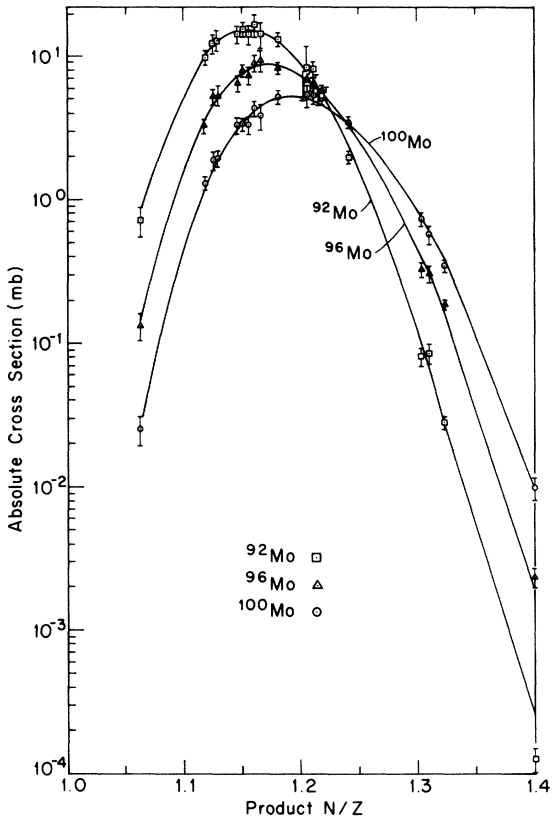

FIG. 1. $A = 72$ isobaric yield distributions in the interaction of 720-MeV α particles with Mo isotopes. The curves represent the skewed Gaussian function (1) fits to the experimental data.

TABLE IV. Parameters of isobaric yield curves of Mo isotopes.

Target	^{92}Mo	^{96}Mo	^{100}Mo
Peak position (N/Z)	1.159 ±0.002	1.181 ±0.001	1.202 ±0.001
FWHM, $\Delta(N/Z)$	0.0983±0.0014	0.1098±0.0010	0.1175±0.0015
Peak height	15.25 ±0.49	8.51 ±0.26	5.23 ±0.15
Skewness γ_1	0.0110±0.0018	0.0156±0.0016	0.0140±0.0014

baric yield curve to be describable by a smooth function, previous works have generally used Gaussian or roughly symmetric curves to describe the shape[2,39,40] as a matter of convenience. However, data generated by the present experiment indicate that the isobaric yield distributions are most definitely not symmetric. The peaks are slightly skewed to the neutron-rich side. Therefore, using a least squares computer program,[41] a skewed Gaussian function was fitted to the cross section data. The formula chosen for the skewed Gaussian distribution is given by the first several terms of the Gram-Charlier A series[42]

$$Y(x)=Y_0\exp(-x^2/2\sigma^2)\left[1+\frac{\gamma_1}{6\sigma}(x^3-3x)+\frac{\gamma_1^2}{72\sigma^2}\times(x^6-15x^4+45x^2-15)\right], \quad (1)$$

where Y_0 is the value at the curve maximum, x denotes N/Z of the product nuclide minus N/Z at the curve maximum $\times(1/\sigma)$, σ is the curve variance, and γ_1 is the skewness.

The χ^2 test showed significant improvement for the fit of the skewed Gaussian over that of a normal Gaussian. The resulting curves are shown in Fig. 1. It is clear from this figure that the skewed Gaussian function satisfactorily describes the isobaric yield curves. The optimally determined parameters of the skewed Gaussian curves are summarized in Table IV.

IV. DISCUSSION

The neutron-to-proton ratios of the initial systems (incident particle plus target nucleus) in this work are 1.182 for ^{92}Mo+α, 1.273 for ^{96}Mo+α, and 1.364 for ^{100}Mo+α. In accordance with the conventional spallation reaction model,[2,7,37] these distinct differences in target composition have a tendency to be smeared out in the cascade and evaporation processes. Figure 2, which schematically represents the average reaction paths of ^{92}Mo and ^{100}Mo, illustrates this point. In the cascade process, the ejection of protons and neutrons from the struck target nucleus depends mostly on the fraction of each originally present. Thus ^{100}Mo has a higher probability of ejecting neutrons than ^{96}Mo and ^{92}Mo, and the average differences of the initial N/Z in the nuclei are somewhat reduced in the nuclear cascade. In the evaporation stage, the relative probability of proton and neutron emission depends largely on the position of the cooling nucleus on the nuclear energy surface. In his theoretical treatment of high temperature evaporation, LeCouteur[43] has shown that the overall effect is a channeling of cooling nuclei toward the minimum of the nuclear energy surface, thus further decreasing the differences among the spectra of spallation products except near the end of the evaporation process when charged particle emission is inhibited by the Coulomb barrier.

Despite the influence of this "channeling effect," an examination of the experimental data in Fig. 1 indicates that the differences in the target nuclei are preserved throughout the reaction. A "memory effect" causes the product yield distribution to be strongly affected by the target composition. There is a gradual shift (only 25% of that of the targets themselves) of the most probable charge toward higher N/Z in going from ^{92}Mo to ^{100}Mo. In addition, the slope on the neutron-richer wing

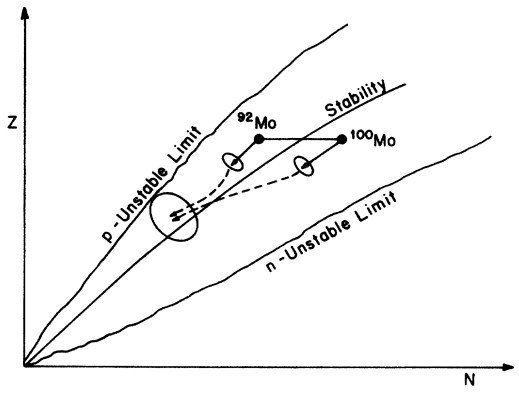

FIG. 2. Schematic representation of the reaction trajectories from ^{92}Mo and ^{100}Mo targets. In spite of the "channeling effect" exerted on the cooling nuclei during the evaporation process by the nuclear energy surface, the spallation products still retain a memory of the composition of the target nuclei. The large separation energies near the p-unstable limit of the nuclear energy surface prohibit the formation of very neutron-deficient species.

decreases (in the negative sense) from ^{92}Mo to ^{100}Mo, thereby broadening the curve for the neutron-richer target as shown by the change of the full width at half maximum (FWHM) listed in Table IV.

The curves in Fig. 1 show another feature of interest. The slopes on the neutron-deficient side of the curves are steeper than the neutron-excess side and remain almost unchanged for the three targets. This trend may be rationalized in terms of the large separation energies of neutrons near the steep slope of the nuclear energy surface (i.e., the proton-unstable limit in Fig. 2) for neutron-deficient nuclei. During the final deexcitation steps, the cooling nuclei are already neutron deficient and further evaporation of neutrons requires a much higher energy than normal. Under these conditions, the emission of charged particles becomes more probable even though the Coulomb barrier hinders their emission at low excitation energy. Formation cross sections for very neutron-deficient products consequently are suppressed. The same argument would hold for proton-deficient products, but since the isobaric yield peaks lie on the neutron-deficient side of stability, the spallation product distributions are yet quite far away from the steep slope of the neutron-unstable side of the nuclear energy surface. As a result, neutron-excessive products are not influenced by the neutron-unstable limit of the nuclear energy surface and are appreciably more sensitive to target composition.

As noted previously by Kaufman[9] the correlation between product yield and target N/Z can be shown more quantitatively in terms of the fractional isobaric yields of the products. A fractional isobaric yield is the ratio of the yield of a particular nuclide to the total (integrated) isobaric yield. These are plotted in Fig. 3 as a function of the N/Z of the initial target system. The neutron-richer products and the neutron-deficient products are shown as solid lines and dashed lines, respectively. In addition to the $A=72$ isobars, several other nuclides whose independent yields have been measured are included. A large difference in the fractional yields is observed when the target N/Z changes. The yields of neutron-richer products increase as the neutron number in the target increases, while the yields of neutron-deficient products decrease. These changes are particularly pronounced for nuclides located far from the maxima of the isobaric yield curves. For instance, the fractional isobaric yield for ^{72}Zn, the most neutron-excessive product we have measured from ^{100}Mo is about 200 times higher than from ^{92}Mo. On the other hand, for nuclides near the peaks of the curves, e.g., ^{72}As, the yields are about the same

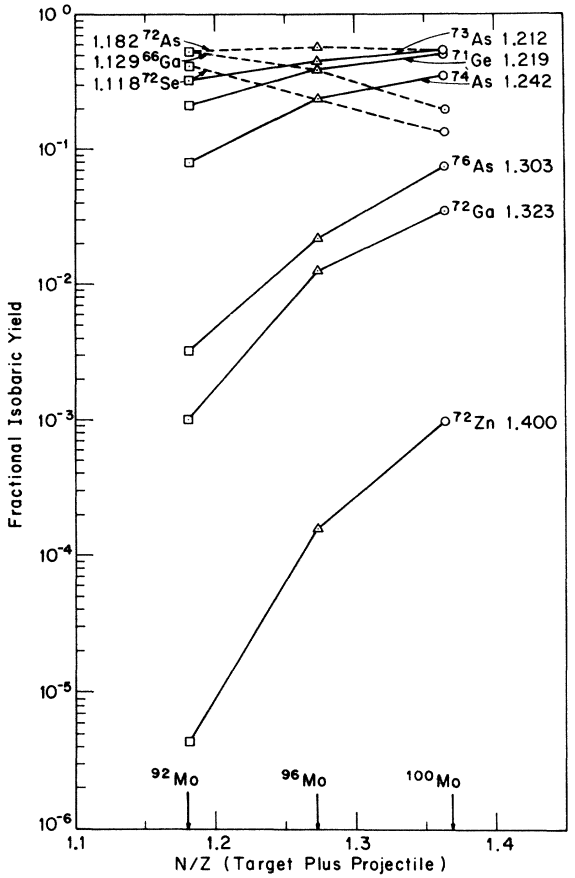

FIG. 3. The variation of the fractional isobaric yield with target composition. The solid lines are for neutron-rich products and the dashed lines for neutron-deficient products. The four-digit numbers represent the neutron-to-proton ratio of each product nuclide.

for the three targets.

The hypothesis proposed by Miller and Hudis,[7] which suggested constant yield ratios for isobaric pairs regardless of target composition, can be examined by studying isobaric yield ratios of the $A=72$ isobars, ^{72}Zn/^{72}Ga, ^{72}Ga/^{72}As, and ^{72}Se/^{72}As, as a function of target N/Z (Fig. 4). The experimental results indicate, contrary to constant ratios, a strong dependence on target composition. For instance, the ratio of ^{72}Ga/^{72}As changes by a factor of almost 30 in going from ^{92}Mo to ^{100}Mo.

Results of the present study may be compared with those obtained in proton-induced spallations, namely, Porile and Church's[10] work in which ^{96}Ru, ^{96}Mo, and ^{96}Zr were irradiated with 1.8-GeV protons and nine radioactive nuclides in the $A \simeq 72$ product mass region ($A=66$–74) were examined. Although the present study is performed at a lower energy but comparable momentum, a comparison with Porile and Church's results should disclose

any similarities and/or differences in the reactions induced by the two types of particles.

Isobaric yield distributions at $A=72$ from 1.8-GeV proton bombardments of ^{96}Ru and ^{96}Zr are displayed in Fig. 5 (solid curves and data points). The 1.8-GeV proton cross sections have been modified slightly from the published values using more recent and reliable decay branching ratios.[44] For purposes of comparison, ^{92}Mo and ^{100}Mo curves from 720-MeV α bombardments are also plotted in Fig. 5 (dashed curves). The proton curves have been *normalized* at the peaks to the α curves to facilitate visual comparison of their shapes from which it is apparent that proton curves exhibit a memory effect similar to that from the present α study. A higher N/Z ratio of the initial target system causes the isobaric yield distribution to displace in the direction of neutron-richer products. Similar to the α curves, these proton curves are asymmetric about the peak and fall more steeply on the neutron-deficient side.

Attempts to fit the skewed Gaussian function (1) to the proton data proved to be unsatisfactory. With only nine data points per target, most of which are located on the center or the neutron-rich side of the curve, a reasonable determination of all four parameters in the skewed Gaussian function was not possible. The curves given in Fig. 5 were taken directly from Ref. 10. It should also be noted that the uncertainties in the proton cross sections are in some cases probably larger than those originally quoted by the authors since their 1964 work was done with NaI(Tl) detectors on cases of overlapping radiations. For example, the 0.835-MeV γ peak of 14-h ^{72}Ga (branching abundance 95.5%) had to be separated from the contributions from 9.5-h ^{66}Ga (branching abundance 5.9%) which has a much higher yield and from 4.9-h ^{73}Ga (branching abundance 2%). This would have undoubtedly introduced a systematic error larger than recognized at the time.

As seen in Fig. 5, the most probable product N/Z of the proton curve and the α curve shows a similar shift as the target composition changes. To illustrate this more quantitatively, the maxima for the α curves (open symbols, from Table IV) and for the proton curves (closed symbols, from Ref. 10, Fig. 7) are plotted together in Fig. 6 as a

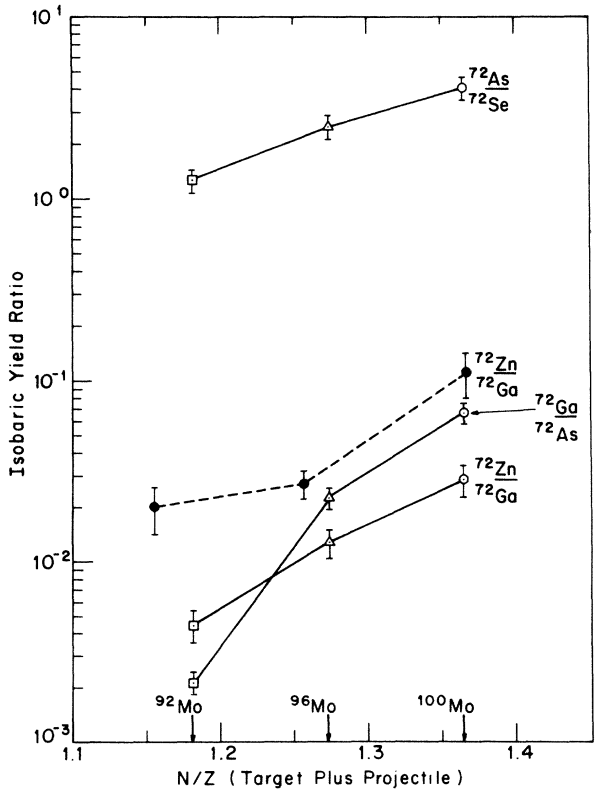

FIG. 4. The variation of the isobaric yield ratio with target composition. The solid curves are for the present α results and the dashed curve for the 1.8-GeV proton results of Ref. 10.

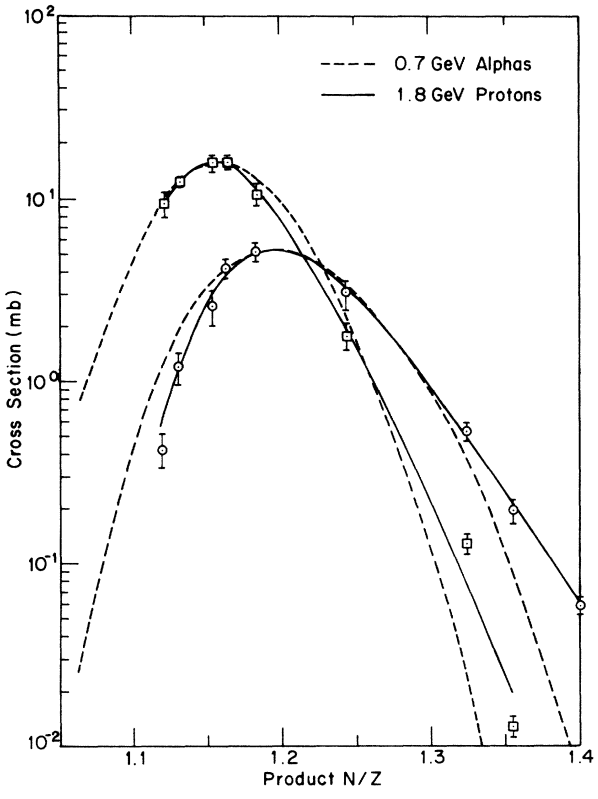

FIG. 5. Comparison of the isobaric yield curves from (Ref. 10) proton (^{96}Ru+p and ^{96}Zr+p) and (this work) α (^{92}Mo+α and ^{100}Mo+α) induced spallations. The proton curves (solid curves with data points) are normalized at the peak to the α curves (dashed curves) to facilitate comparisons of their shapes.

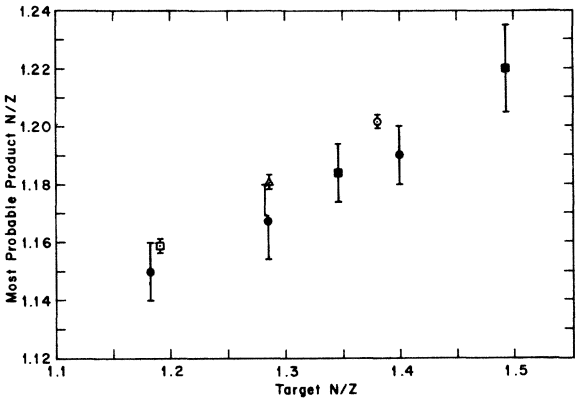

FIG. 6. The variation of the most probable product N/Z with target N/Z. Open symbols represent the present α results (^{92}Mo, ^{96}Mo, and ^{100}Mo) and filled symbols represent the proton results from (Ref. 10) Porile and Church (^{96}Ru, ^{96}Mo, and ^{96}Zr) and (Ref. 9) Kaufman (In and Au).

function of target N/Z. Also included in the figure are the peak position data for In and Au targets obtained from Kaufman's 2.9-GeV proton work.[9] Since less data are available for proton isobaric yield curves, their peaks are somewhat less well defined as reflected in the relatively larger error bars.

It was found that a nearly linear relationship is obtained when the "target plus projectile N/Z" is used as abscissa (Fig. 7) instead of just "target N/Z." This suggests the interesting speculation that one can use an overall master curve to fit data of spallation reactions for all types of incident particles, provided that the projectile composition is

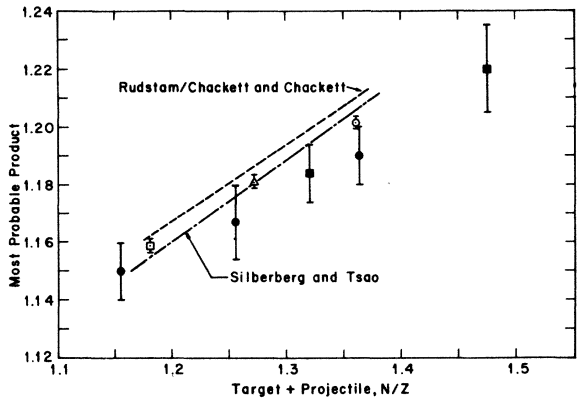

FIG. 7. The variation of the most probable product N/Z with "target plus projectile N/Z." Open symbols represent the present α results (^{92}Mo, ^{96}Mo, and ^{100}Mo) and filled symbols represent the proton results (Ref. 10) from Porile and Church (^{96}Ru, ^{96}Mo, and ^{96}Zr) and (Ref. 9) Kaufman (In and Au). The lines represent predictions from empirical formulas by Chackett and Chackett (dashed) (Ref. 13) and Silberberg and Tsao (dash-dot) (Ref. 39).

taken into consideration. Sparse existing data are consistent with this observation. Comparison of copper spallation[18] by 720-MeV α particles and 590-MeV protons showed a similar effect but expressed as a relative suppression of very neutron-deficient products from α spallation. N/Z for "target plus projectile" here are 1.194 and 1.167, respectively. Spallation of copper[36,37] by 3.9-GeV ^{14}N and 25-GeV ^{12}C with "target plus projectile" N/Z's of 1.167 and 1.171 shows no such distinction from proton spallations in concordance with the suggested relationship. However, since the present α and proton data are too limited to establish the validity of this hypothesis, further experimental evidence using other projectiles is needed.

In addition to the peak shift, a variation in width (primarily on the neutron-rich side) has been observed in the present α study. It is seen in Fig. 8 that the FWHM (open symbols) and full width at tenth maximum (FWTM) (filled symbols) of the isobaric yield curves increase with increasing target N/Z. The observed enhancement for neutron-richer species may be attributed to both a shift in yield maximum and an increase in curve width. A similar broadening phenomenon had been reported in a proton study made by Thibault-Philippe.[14] In the latter study, ^{92}Mo and ^{100}Mo were bombarded with 25-GeV protons and the cross sections of nine sodium isotopes (^{21}Na to ^{29}Na) were measured. The isotopic yield distributions, which also indirectly reveal the trends of isobaric yield distributions, exhibit an analogous increase in width on the neutron-rich side from ^{100}Mo (Fig. 32, Ref. 14).

It is worthwhile to point out that in the proton work of Porile and Church,[10] these authors reported that the FWHM remains fairly constant for the three targets studied (^{96}Zr, ^{96}Mo, and ^{96}Ru), implying that the striking enhancement of neutron-rich nuclide formation from neutron-rich targets

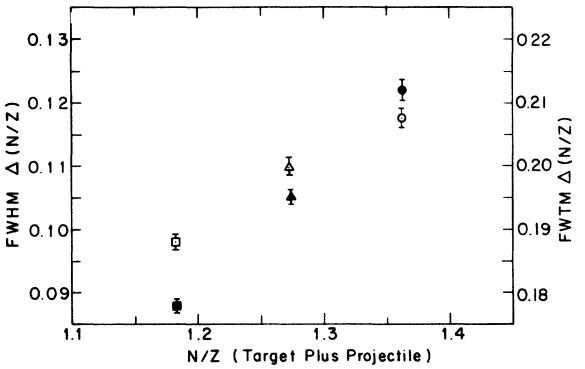

FIG. 8. The variation of the width of the $A = 72$ isobaric yield curve with target composition. FWHM (full width at half maximum), open symbols; FWTM (full width at tenth maximum), filled symbols.

is caused entirely by a displacement of the peak position without altering the curve shape. A detailed reexamination of their data, however, confirms that a change in slope on the neutron-rich wing actually does exist. The trend can be clearly displayed by the change in the ^{72}Zn/^{72}Ga ratio for the three targets. ^{72}Zn and ^{72}Ga are especially suitable for this purpose since they are both situated far away from the peak. As a consequence their ratio provides a sensitive test for the variation of the slope of the neutron-rich wing. If the shape of the curve remains unaltered for the three targets, then a constant ratio should be obtained. The ^{72}Zn/^{72}Ga ratios of the proton study (Ref. 10, Table IV) are reproduced as the dashed curve in Fig. 4. It is plainly evident that an increase in the ^{72}Zn/^{72}Ga ratio, and therefore an increase in width, is associated with an increase in target N/Z. One therefore concludes that the effect of target composition on the product isobaric yield distributions is very much the same in α-induced spallation as it is in proton-induced spallation.

Several empirical formulas[13,39,40] have been proposed initially by Rudstam and subsequently by various other authors for estimating the production cross sections of proton-induced spallation.

The semiempirical formula as originally constructed by Rudstam[39] has the following form:

$$\sigma(Z,A)=f(A_t)f(E)\exp(PA-R\left|Z-SA+TA^2\right|^{3/2}),$$

where Z, A equals Z, A of the product nuclide, A_t is the target mass number, E is the bombardment energy, and P, R, S, T are constants.

The detailed physical significance of the individual terms in this expression is discussed in Ref. 39. The term $R\left|Z-SA+TA^2\right|^{3/2}$ is related to the isobaric yield distribution. The width of the distribution is represented by the parameter R (for $A=72, R=1.7222$). The location of the peak of the distribution is defined by parameters $S(=0.486)$ and $T(=0.00038)$. It is apparent that Rudstam's formula not unexpectedly fails to accommodate the present α results since in this formula the isobaric yield distribution is dependent only on the product nucleus. An invariant distribution results from targets with different N/Z ratios. Indeed, Rudstam's formula has been found useful mostly for targets close to the stability line[38] which is not surprising since it was parametrized around results from such targets.

An improved empirical formula which takes into account the target composition has been developed by Chackett and Chackett.[13] In this equation, the constant S in Rudstam's formula is replaced by a simple expression involving the target composition:

$$S'=S_0-U'(A_t/Z_t)+V'A_t,$$

where A_t, Z_t equals A, Z of the target nucleus, $U'=0.006$, $V'=0.00005$, and $S_0=0.616$.

The empirically calculated isobaric yield distributions, normalized at the peak, for ^{92}Mo and ^{100}Mo using this relationship are shown with the experimental data in Fig. 9. In the calculation for α-induced spallation, the A_t and Z_t employed were the combined values of target plus α particle. By including the projectile composition in the computations, as done here, the calculated data fit the experimental data better than when considering the target alone.

An alternate empirical formula which also includes target composition in the computations has been proposed by Silberberg and Tsao.[39] In this formula, the Rudstam constant S is replaced by

$$S''=S-0.06(A_t-\bar{A}_t)/Z_t,$$

where $S=0.486$ and $\bar{A}_t$ denotes the mass number corresponding to the mean of the stable isotopes of a given atomic number. Again it is found that the best agreement with experimental data is obtained when the projectile composition is taken into consideration in A_t. The results from this equation, also normalized at the peak, are likewise shown in Fig. 9. Several observations can be made from a comparison of the calculated and experi-

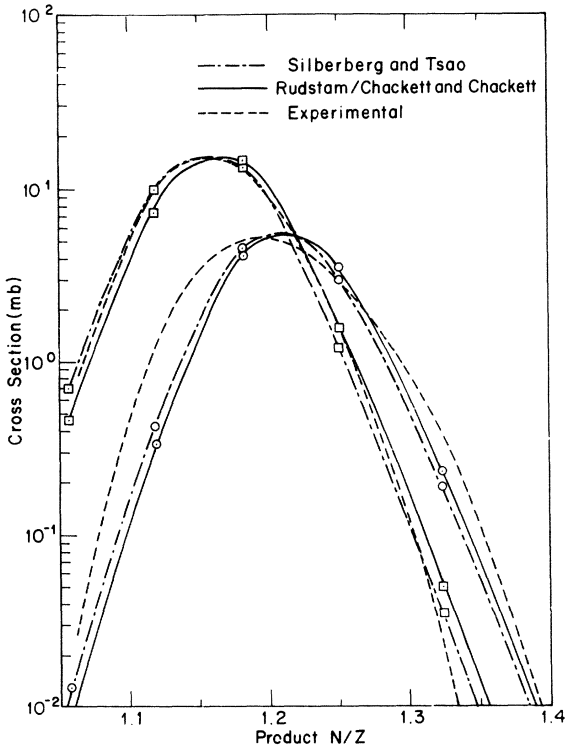

FIG. 9. Comparison of experimental data with empirical formulas for ^{92}Mo and ^{100}Mo. The calculated curves are normalized at the peak to the experimental curves.

mental curves in this figure. The results from the two empirical formulas are almost identical. Both effectively predict the shift in peak position for targets with different N/Z ratios. However, the change in width of the curves is not reproduced by these computations. This disagreement is due to the fact that in the empirical formulas, a constant R (=1.7222), instead of a parameter which reflects target composition, is used for all targets. The theoretically calculated peak positions are plotted in Fig. 7 (dashed lines). The narrower distribution for ^{100}Mo predicted by the formulas (see Fig. 9) tends to displace the most probable product toward a higher N/Z value, resulting in a steeper increase for the calculated maxima than experimentally observed. Furthermore, these formulas use a symmetric function, namely $\exp(-R\,|Z - S'A + TA^2|^{3/2})$, to describe the isobaric yield distribution, which is in contradiction to the observed asymmetric distributions.

The discrepancies between experiment and semiempirical predictions can be understood when one recalls that parameters for the latter were adjusted to existing spallation data, the majority of which are confined to relatively long-lived radionuclides. These, of course, are mostly close to stability which in turn places them at the peak and slightly neutron rich of the peak in the isobaric yield distribution. From Fig. 2, it is seen that such nuclei, upon which Rudstam-like formulas are parametrized, are *least* sensitive to target composition. The current investigation has extended measurements beyond these products. Clearly, a better fit can be obtained when a more realistic function, such as the skewed Gaussian function, is used to describe isobaric yield distributions.

The authors wish to acknowledge the cooperation and hospitality of Dr. Robert T. Siegel and the SREL staff. Appreciable gratitude is extended to Dr. Richard L. Klobuchar and Ms. H. S. Hwang for assistance with computational data analysis. One of the authors (THK) acknowledges partial support of the U.S.A.E.C. during the research period.

*Present address: Department of Applied Sciences, Brookhaven National Laboratory, Upton, New York 11973.

[1]*High-Energy Nuclear Reactions in Astrophysics*, edited by B. S. P. Shen (Benjamin, New York, 1967).
[2]*Spallation Nuclear Reactions and Their Applications*, edited by B. S. P. Shen (Reidel, Boston, 1976).
[3]L. G. Stang, Jr., M. Hillman, and E. Lebowitz, Brookhaven National Laboratory Report No. 50195 (T-547), 1969 (unpublished).
[4]B. R. Erdal, P. M. Grant, V. R. Casella, A. E. Ogard, and H. A. O'Brien, Jr., NBS Special Publication No. 425, 1975 (unpublished), p. 492.
[5]R. Serber, Phys. Rev. 72, 1114 (1947).
[6]M. L. Goldberger, Phys. Rev. 74, 1269 (1948).
[7]J. M. Miller and J. Hudis, Annu. Rev. Nucl. Sci. 9, 159 (1959).
[8]I. Dostrovsky, P. Rabinowitz, and R. Bivins, Phys. Rev. 111, 1659 (1958).
[9]S. Kaufman, Phys. Rev. 129, 1866 (1963).
[10]N. T. Porile and L. B. Church, Phys. Rev. 133, B310 (1964).
[11]G. Friedlander and L. Yaffe, Phys. Rev. 117, 578 (1960).
[12]G. N. Simonoff and C. Vidal, Phys. Lett. 20, 30 (1966).
[13]K. F. Chackett and G. A. Chackett, Nucl. Phys. A100, 633 (1967).
[14]C. Thibault-Philippe, Doctoral Dissertation, University of Paris, 1971 (unpublished).
[15]M. Lagarde, Doctoral Dissertation, Bordeaux University, France, 1972 (unpublished).
[16]M. Lagarde-Simonoff, S. Regnier, H. Sauvageon, G. N. Simonoff, and F. Brout, J. Inorg. Nucl. Chem. 37, 627 (1975).
[17]R. Korteling and E. J. Hyde, Phys. Rev. 136, B425 (1964).
[18]P. J. Karol, Phys. Rev. C 10, 150 (1974).
[19]A. M. Zebelman, A. M. Poskanzer, J. D. Bowman, R. G. Sextro, and V. E. Viola, Jr., Phys. Rev. C 11, 1280 (1975).
[20]P. J. Karol and J. M. Miller, Phys. Rev. 166, 1089 (1968).
[21]D. J. Reuland and A. A. Caretto, Jr., Nucl. Phys. A151, 449 (1970).
[22]W. J. Nieckarz, Jr. and A. A. Caretto, Jr., Phys. Rev. C 3, 1921 (1970).
[23]R. F. Schall, Jr. and A. A. Caretto, Jr., Phys. Rev. C 3, 1924 (1970).
[24]SREL is supported by the National Aeronautics and Space Administration, Commonwealth of Virginia, and the National Science Foundation.
[25]T. H. Ku and P. J. Karol, Nucl. Instrum. Methods 121, 537 (1974).
[26]S. Kaufman, Phys. Rev. 126, 1189 (1962).
[27]J. Stary, *The Solvent Extraction of Metal Chelates* (MacMillan, New York, 1965), p. 195.
[28]National Academy of Sciences-Nuclear Science Series Report No. NAS-NA-3111, 1970 (unpublished).
[29]J. B. Cumming, National Academy of Sciences-Nuclear Science Series Report No. NAS-NA-3107, 1962 (unpublished).
[30]R. D. Meeker and A. B. Tucker, Nucl. Phys. A157, 337 (1970).
[31]Y. Y. Chu, E. M. Franz, and G. Friedlander, Phys. Rev. C 10, 156 (1974).
[32]H. G. Hicks and R. S. Gilbert, Phys. Rev. 100, 1286 (1955).
[33]C. M. Lederer, J. M. Hollander, and I. Perlman, *Table of Isotopes* (Wiley, New York, 1967), 6th ed.
[34]K. R. Alvar, Nucl. Data Sheets 11, 121 (1974).
[35]K. R. Alvar, Nucl. Data Sheets 10, 205 (1973).
[36]J. B. Cumming, P. E. Haustein, R. W. Stoenner,

L. Mausner, and R. A. Naumann, Phys. Rev. C 10, 739 (1974).
[37]J. B. Cumming, R. W. Stoenner, and P. E. Haustein, Phys. Rev. C 14, 1554 (1976).
[38]J. Hudis, in *Nuclear Chemistry*, edited by L. Yaffe (Academic, New York, 1968), Chap. 3, p. 169.
[39]G. Rudstam, Z. Naturforsch. 21a, 1027 (1966).
[40]R. Silberberg and C. H. Tsao, Astrophys. J. Suppl. 25, 313 (1973); 25, 335 (1973).
[41]R. L. Klobuchar (private communication).
[42]*Handbook of Mathematical Functions*, edited by M. Abramowitz and I. Segun (Dover, New York, 1968), p. 935.
[43]K. LeCouteur, in *Nuclear Reactions*, edited by P. M. Endt and M. Demeur (North-Holland, Amsterdam, 1959), Vol. I, Chap. 7.
[44]W. W. Bowman and K. W. MacMardo, At. Data Nucl. Data Tables 13, 211 (1974).